Optimal Design of NRD Grating Bandpass Filters for THz Application Using GA and EIM

Md. Iquebal Hossain Patwary, Akito Iguchi, *Member, IEEE*, and Yasuhide Tsuji, *Senior Member, IEEE*

***Abstract*—Compact and low-loss waveguide devices are highly desired in the development of THz-wave circuits. Nonradiative dielectric (NRD) waveguides having simple structures and very low loss are promising platforms for THz-wave circuits, and previously some basic devices have been reported. As the NRD guide has a non-radiative nature, the NRD grating bandpass filters that have been reported for millimeter-wave circuits are more suitable to design in THz-wave range. In this paper, we present THz NRD grating bandpass filters and develop an efficient optimal design method to realize these devices based on genetic algorithm (GA) and effective index method (EIM). The optimized device achieved the desired flat top transmission band within the aimed frequency range with only 0.46 dB of avg. IL in the passband, where the reflection in the passband is better than −20 dB. The results obtained with EIM are also verified by three-dimensional finite element method (3D-FEM). The fabrication tolerance of the proposed devices has also been discussed in detail.**

***Index Terms*—Nonradiative dielectric waveguide, grating bandpass filter, genetic algorithm, effective index method, full-vectorial finite element method, three-dimensional finite element method.**

I. Introduction

THE usage of THz technology [1] is actively being explored due to its potential applications in numerous scientific and technological fields, such as biotechnology [2], [3], telecommunication [4], [5], spectroscopy [6] and imaging [7], [8], [9]. However, wave guiding in the THz region still remains challenging and the conventional waveguides used in other frequency bands exhibit significant transmission loss over a long distance in this frequency spectrum. To meet the demand for suitable THz waveguides, several waveguides have been proposed over the past few years, including metallic waveguides [10], [11], parallel plate dielectric waveguides (PPDW) [12], [13] and non-radiative dielectric waveguides (NRD) [14], [15]. As the THz-wave circuit development needs the use of compact and low-loss waveguide devices, NRD guides are drawing significant attention for THz-wave integrated circuits due to their simple structures and very low loss over a long distance in the THz region. NRD guide with non-radiative nature has a structure consists of a dielectric strip placed between two parallel metal plates with spacing less than $\lambda/2$ and supports LSM and LSE modes as shown in Fig. 1.

Manuscript received 25 September 2023; revised 11 November 2023; accepted 16 December 2023. Date of publication 19 December 2023; date of current version 29 December 2023. This work was supported by JSPS (Japan) KAKENHI under Grant 21K04169. *(Corresponding author: Yasuhide Tsuji.)*

The authors are with the Muroran Institute of Technology, Muroran 060-8585, Japan (e-mail: y-tsuji@mmm.muroran-it.ac.jp).

Digital Object Identifier 10.1109/JPHOT.2023.3344608

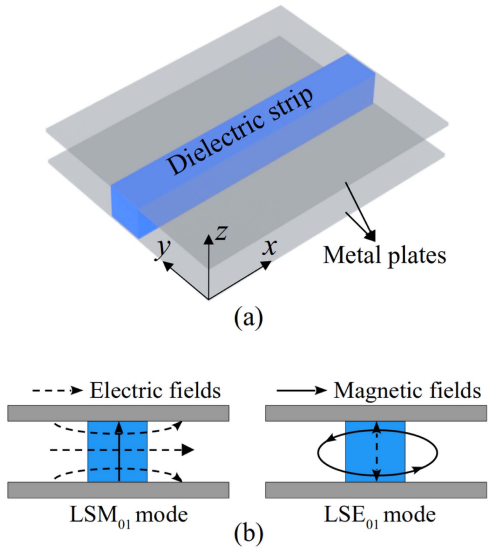

Fig. 1. (a) 3D model of the NRD guide, (b) NRD propagation modes.

In the development of THz-wave integrated circuits, bandpass filters serve as crucial components and several kinds of bandpass filters based on different device types, including metal waveguide, plasmonic waveguide, photonic crystals, frequency selective surfaces (FSS), metamaterials, and metasurfaces, have been presented so far [16], [17], [18], [19], [20], [21], [22], [23], [24] for various THz circuit applications. NRD grating bandpass filters have been proposed for millimeter-wave integrated circuits by T. Yoneyama [25]. After that, many researchers have discussed these grating filters over the last few decades [26], [27], [28], [29], but all of these filters have been designed in millimeter-wave range where the conductor loss of the waveguide can be negligible. In THz range where conductor loss is not negligible, the design of these filters and the design methodology to realize these filters have not been well-discussed yet. Moreover, as NRD guide confines almost all the power inside the dielectric strip, the NRD grating bandpass filters appear to be more appropriate to design in THz-wave range. Therefore, the design of THz NRD grating bandpass filters and an efficient optimal design method to realize these grating devices are crucial considering the conductor loss of the waveguide.

In this paper, we propose NRD grating bandpass filters for THz-band circuit applications and an efficient optimal design method based on genetic algorithm (GA) and effective index

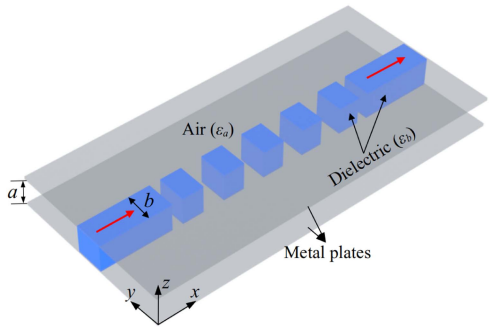

Fig. 2. Design model of NRD grating bandpass filter.

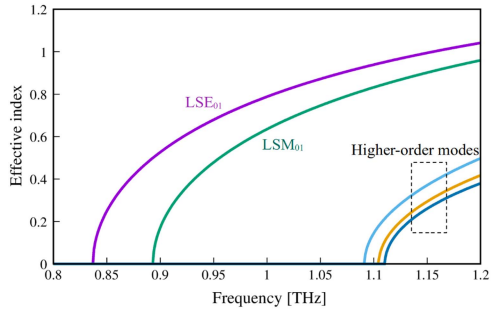

Fig. 3. Dispersion relation for $a = b = 135$ μm and $\varepsilon_b = 2.3$ (polyethylene).

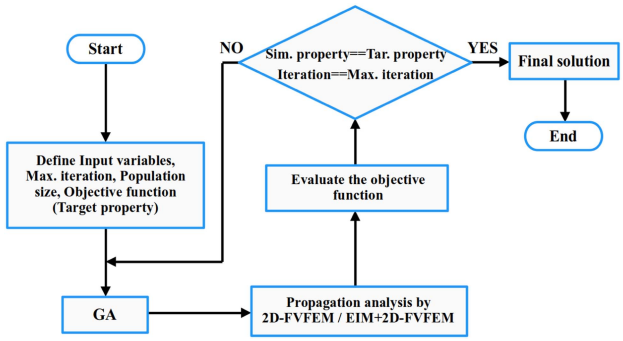

Fig. 4. Flowchart of optimal design process of NRD grating bandpass filters using GA and EIM.

method (EIM) to design these filters. GA is used as an optimization method to find the optimal solution globally, and EIM is employed to calculate the conductor loss of the proposed THz-band filters. Here, for the propagation analysis of the grating filters we employ recently developed two-dimensional full-vectorial finite element method (2D-FVFEM) for NRD guide devices [30]. In this research, initially we design several THz bandpass filters, single pass-band bandpass filter, frequency-tunable bandpass filter, and bandwidth-tunable bandpass filter by using GA where conductor plates are considered as perfect electric conductor (PEC). As the conductor loss of the waveguide is not negligible, we show the practial application of these designed filters by estimating the conductor loss using EIM combined with 2D-FVFEM in the optimization process. In this case, the conductor plates are considered to be silver (Ag), and single pass-band bandpass filter is considered to be optimized again with GA and EIM. Here, all the device lengths are nearly identical and obtained almost ideal transmission property by 2D-FVFEM, thus the conductor loss will be the same for the other design examples as well. Then, the obtained transmission property from the EIM and 2D-FVFEM is confirmed by 3D-FEM. Finally, we show the fabrication tolerance of these devices in terms of parameters deviation effect on the bandwidth and central frequency of the designed filters.

II. Optimal Design Method of NRD Grating Bandpass Filters

In this research, we consider a design model of THz NRD grating bandpass filter as shown in Fig. 2. Here, the spacing between metal plates and width of the dielectric strip are considered to be, $a = b = 135$ μm. Polyethylene is considered as the dielectric material whose relative permittivity is $\varepsilon_b = 2.3$ and $\varepsilon_a = 1$ is considered as the air permittibity. Polyethylene has been widely used in THz systems because of the advantages of low absorption loss, low refractive index and high rigidity [31]. Furthermore, NRD guide with polyethylene as dielectric material has a very low transmission loss at THz frequencies [32]. Here, LSM_{01} mode is used in NRD as the guided mode and operating region for the proposed NRD filters is considered from 0.9 THz to 1.1 THz. Fig. 3 shows the dispersion relation around 1 THz for $a = b = 135$ μm and $\varepsilon_b = 2.3$, where maximum single mode operation band for LSM_{01} mode is obtained at the targeted operating region and at the higher frequency side outside the operating region, transmission may deteriorate due to the appearance of the higher-order modes. The flowchart of the optimization process is illustrated in Fig. 4. Initially, the design variables, objective function that is the target property, maximum iteration and population size for the GA are to be set. Here, the length of the dielectric block and air gap are considered as the design variables, and in the optimization process, maximum 100 of iterations are evaluated and population size is defined $N_p = 48$. Then, optimization of the design variables is carried out using GA, and during the process the propagation in the NRD devices is efficiently analyzed by the 2D-FVFEM or EIM+2D-FVFEM (in case of conductor loss consideration) and evaluating the objective function. The process is continued untill the simulated transmission property is equal to the target transmission property or the number of iterations reach to the maximum iteration. Finally, after the optimization process, an optimized NRD grating filter with desired characteristics in the THz region can be obtained.

A. Optimization With GA

In this study, the design variables are efficiently optimized by utilizing GA. GA is the method for solving optimization problems based on natural selection [33], the process that drives biological evolution. It is a versatile design approach and is widely used in various design problems. In GA, the initial individuals are randomly generated, and genetic operations such

as selection, crossover, and mutation are repeated until the desired characteristics are obtained. The selection methods include ranking selection where individuals with high fitness are selected to succeed their genetic information to the next generation and those with low fitness are eliminated, and elite selection that is leaving highly adapted individuals to the next generation as they are. In this study, ranking selection and elite selection are used together to keep the diversity of the solution search. Then, the new children, x_c^{n+1}, in the next generation are generated by the crossover of the two selected parents, x_{p1}^n and x_{p2}^n, according to the following equation.

$$x_{c,i}^{n+1} = w x_{p1,i}^n + (1-w) x_{p2,i}^n \tag{1}$$

where w is the weight coefficient and is given as the random number $(w \in [0,1])$, and i is the i-th component of the genetic information vector. Here, the mutation is the process of randomly mutating the genetic information of individuals by a given probability to ensure diversity of the solution and to avoid falling into a local solution. In this study, the mutation rate is set to 3%.

B. Propagation Analysis by 2D-FVFEM

A propagation field in the given devices is simulated by 2D-FVFEM during the optimization process. Considering the three-dimensional structure of the NRD grating filters as illustrated in Fig. 2 is uniform along the z-direction and the direction of light propagation is in the xy-plane. Then, the functional of propagating behavior for the NRD devices can be expressed as follows:

$$F = \iiint \left[(\nabla \times \mathbf{\Psi}^*) \cdot \left(\frac{1}{\varepsilon_r} \nabla \times \mathbf{\Psi} \right) - k_0^2 \mathbf{\Psi}^* \cdot \mathbf{\Psi} \right] dV - \iint \left\{ \mathbf{\Psi}^* \cdot \left(\boldsymbol{i}_n \times \frac{1}{\varepsilon_r} \nabla \times \mathbf{\Psi} \right) \right\} dS \tag{2}$$

where k_0 is a free-space wavenumber, ε_r is a relative permittivity distribution and $\mathbf{\Psi} = \boldsymbol{H}$. Here, each component of $\boldsymbol{H}$ can be expressed as follows:

$$H_x = \psi_x(x,y) \cos\left(\frac{\pi}{a} z\right) \tag{3}$$

$$H_y = \psi_y(x,y) \cos\left(\frac{\pi}{a} z\right) \tag{4}$$

$$H_z = \psi_z(x,y) \sin\left(\frac{\pi}{a} z\right) \tag{5}$$

Discretizing computational region into edge/nodal hybrid triangular elements [34], [35], and substituting (3), (4) and (5) into the functional (2), the final linear equation of FEM can be derived as follows:

$$\left([K] - k_0^2 [M] \right) \{\psi\} = [P] \{\psi\} = \{u\} \tag{6}$$

where $[P]$ is a FEM matrix, $\{\psi\}$ is a discretized field and $\{u\}$ is an incidence condition.

The LSM mode in the input port can be treated by the (6) derived from the full-vectorial expression (2), and is obtained by solving the following wave equation:

$$\frac{\partial}{\partial y} \left(\frac{1}{\varepsilon_r} \frac{\partial \psi_z}{\partial y} \right) + \left(k_0^2 - \frac{\beta^2 + (\pi/a)^2}{\varepsilon_r} \right) \psi_z = 0 \tag{7}$$

where β is the propagation constant of LSM mode.

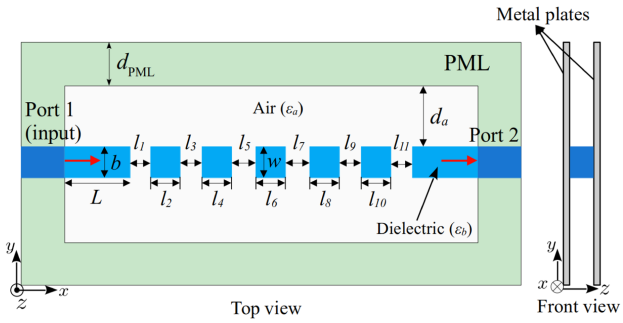

Fig. 5. Design model of THz NRD grating single pass-band bandpass filter.

III. Design Examples of NRD Grating Bandpass Filters

We show the validity of the optimal design method for THz NRD grating filters by designing several bandpass filters, single pass-band bandpass filter, frequency-tunable bandpass filter, and bandwidth-tunable bandpass filter. This section presents the design and optimized results of these grating filters.

A. Single Pass-Band Bandpass Filter

First, we consider the design problem of a single pass-band bandpass filter with five dielectric blocks as shown in Fig. 5. The structure is symmetric in x- and y-direction, where $w = b = 135\ \mu$m, $l_1 = l_{11}$, $l_3 = l_9$, $l_5 = l_7$, and $l_2 = l_4 = l_6 = l_8 = l_{10}$. Therefore, the design variables for this design problem are, l_1, l_2, l_3 and l_5. The range of the design variables in the optimization process are set to, $l_1 = l_3 = 20\ \mu\text{m} \sim 100\ \mu\text{m}$ and $l_2 = l_5 = 20\ \mu\text{m} \sim \lambda/2$, where $\lambda = 300\ \mu$m (wavelength at 1 THz). Perfectly matched layer (PML) is considered around the computational domain with a thickness of $d_{\mathrm{PML}} = 250\ \mu$m. The length of the input/output ports, and the distance between the dielectric and PML along y-axis are set to be $L = d_a = 250\ \mu$m. LSM_{01} mode is incident to the input port 1. The passband is assumed to be 48 GHz from 0.976 THz to 1.024 THz to get a flat top transmission band around the central frequency 1 THz. The objective function to be minimized is given by

$$\text{Minimize } C = C_1 + C_2 + C_3 \tag{8}$$

$$C_1 = \sum_{f=f_1}^{f_2} \left[|S_{21}(f)|^2 + \left(1 - |S_{11}(f)|^2 \right) \right]$$

$$C_2 = \sum_{f=f_3}^{f_4} \left[W\,|S_{11}(f)|^2 + \left(1 - |S_{21}(f)|^2 \right) \right]$$

$$C_3 = \sum_{f=f_5}^{f_6} \left[|S_{21}(f)|^2 + \left(1 - |S_{11}(f)|^2 \right) \right]$$

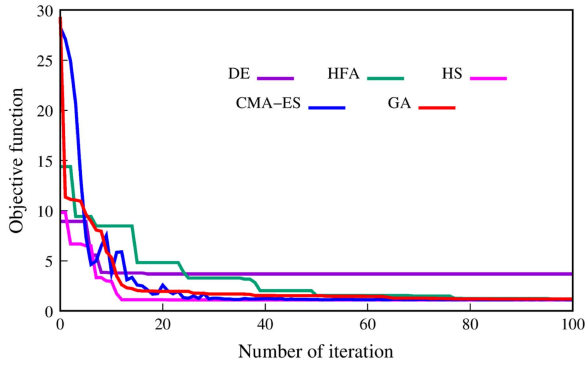

Fig. 6. Convergence behavior in the optimal design of single pass-band bandpass filter using GA and other existed optimization methods.

TABLE I
RANGE OF DESIGN VARIABLES AND OPTIMIZED PARAMETERS OF THE DESIGNED BANDPASS FILTER (BW = 48 GHz, CF = 0.9995 THz)

Design variable	Variable range	Optimized parameter
l_1	20 μm $\sim$ 100 μm	42.556 μm
l_2	20 μm $\sim$ λ/2	125.025 μm
l_3	20 μm $\sim$ 100 μm	98.807 μm
l_5	20 μm $\sim$ λ/2	117.391 μm

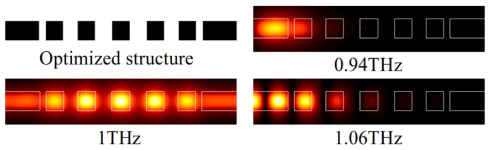

Fig. 7. Optimized structure and propagation fields in the optimized bandpass filter at different frequencies within passband and rejection band (BW = 48 GHz, CF = 0.9995 THz).

where $|S_{21}|^2$ is maximized and $|S_{11}|^2$ is minimized inside the passband, and in the rejection band, $|S_{21}|^2$ is minimized and $|S_{11}|^2$ is maximized. W is the weight coefficient considered to minimize the return loss in the passband and is set to be 1. Here, $f_1 = 0.92$ THz, $f_2 = 0.97$ THz, $f_3 = 0.976$ THz, $f_4 = 1.024$ THz, $f_5 = 1.03$ THz and $f_6 = 1.08$ THz. 22 frequencies are considered at the rejection band regions from 0.92 THz to 0.97 THz and 1.03 THz to 1.08 THz with an interval of 0.005 THz, and 25 frequencies are considered in the the passband from 0.976 THz to 1.024 THz with an interval of 0.002 THz to considerably suppress the unwanted resonance and get a flat top transmission. The convergence behavior of the objective function in the device optimization is depicted in Fig. 6. Here, we compare the device optimization using GA with other existed optimization methods, such as, Differential evolution (DE), Hybrid firefly algorithm (HFA), Harmony search (HS) [36] and Covariance matrix adaptation evolution strategy (CMA-ES) [37] in terms of convergence behavior of the objective function. Although, except DE all the optimization methods show almost the same convergence behavior, GA is used in this paper due to its wide usability in various design problems and is very simple to use compared to the other optimization methods. The optimized parameters of the designed bandpass filter are shown in Table I. Fig. 7

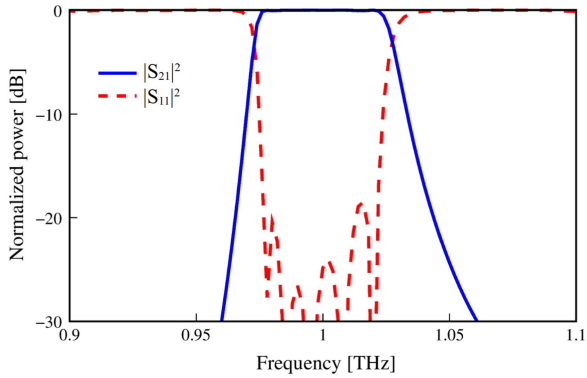

Fig. 8. Frequency characteristics of the optimized bandpass filter (BW = 48 GHz, CF = 0.9995 THz).

shows the optimized structure of the single pass-band bandpass filter and the propagation fields in the optimized structure for different frequencies within the passband region as well as in the rejection band region. We can see, the frequency within the passband is transmitted through the device and the frequencies in the rejection band are greatly rejected by the optimized structure. The frequency characteristics curve is depicted in Fig. 8, which illustrates that the optimized bandpass filter achieved the desired flat top transmission property at the targeted frequency band with the optimized central frequency (CF) of 0.9995 THz. Here, the optimized bandpass filter achieved the targeted passband of 48 GHz with a 0.45-dB bandwidth and 99.6% of average transmission power, thus 0.45-dB bandwidth is taken as a reference in this paper for all the optimized bandwidth (BW) consideration.

B. *Frequency-Tunable Bandpass Filter*

In addition to the specific frequency filter, it is expected to achieve frequency-tunable bandpass filter due to their potential applications in the THz integrated circuits [38], [39], [40], [41]. Therefore, we consider the design problem of THz frequency-tunable bandpass filter with the same design model shown in Fig. 5. Here, the target bandwidths are set to be 48 GHz, the target central frequencies of the bandpass filter are considered to be 0.98 THz, 1.02 THz and 1.04 THz, and adjusted in the optimization process. For 0.98 THz and 1.02 THz, range of the design variables and the weight coefficient W in the objective function are same as the design example of 1 THz. In case of 1.04 THz, design variables are set to, $l_1 = l_3 = 20$ μm $\sim$ λ/2 and $l_2 = l_5 = 20$ μm $\sim$ 200 μm, and W is set to be 5. The other design parameters are left unchanged from the previous design example. Table II shows the optimized parameters of the designed bandpass filter at different optimized central frequencies. After optimization, the obtained central frequencies are, 0.9811 THz, 1.019 THz and 1.0395 THz with the optimized bandwidths of, 49 GHz, 47 GHz and 48 GHz, respectively. The optimized structure of the bandpass filter at different central frequencies and the propagation fields within the passband and rejection band are shown in Fig. 9. We can see the devices designed at different central frequencies accomplish the bandpass filtering function with almost desired transmission and rejection in the passband

TABLE II
RANGE OF DESIGN VARIABLES AND OPTIMIZED PARAMETERS OF THE DESIGNED FREQUENCY-TUNABLE BANDPASS FILTER AT CENTRAL FREQUENCY, 0.9811 THZ, 1.019 THZ AND 1.0395 THZ

Design variable	Variable range	Optimized parameter
BW = 49 GHz, CF = 0.9811 THz		
l_1	20 μm $\sim$ 100 μm	30.998 μm
l_2	20 μm $\sim$ $\lambda/2$	149.998 μm
l_3	20 μm $\sim$ 100 μm	75.515 μm
l_5	20 μm $\sim$ $\lambda/2$	93.444 μm
BW = 47 GHz, CF = 1.019 THz		
l_1	20 μm $\sim$ 100 μm	32.966 μm
l_2	20 μm $\sim$ $\lambda/2$	103.314 μm
l_3	20 μm $\sim$ 100 μm	99.969 μm
l_5	20 μm $\sim$ $\lambda/2$	133.455 μm
BW = 48 GHz, CF = 1.0395 THz		
l_1	20 μm $\sim$ $\lambda/2$	24.263 μm
l_2	20 μm $\sim$ 200 μm	85.438 μm
l_3	20 μm $\sim$ $\lambda/2$	94.691 μm
l_5	20 μm $\sim$ 200 μm	144.591 μm

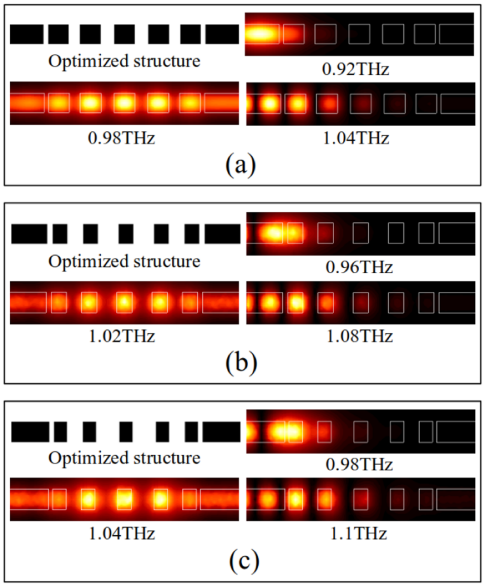

Fig. 9. Optimized structure and propagation fields in the optimized bandpass filter at different frequencies within passband and rejection band, (a) BW = 49 GHz and CF = 0.9811 THz, (b) BW = 47 GHz and CF = 1.019 THz, and (c) BW = 48 GHz and CF = 1.0395 THz.

and rejection band, respectively. Fig. 10 illustrates the frequency characteristics of the designed frequency-tunable bandpass filter, where we can see the devices achieved the desired flat top transmission property at the targeted frequency band for the different central frequencies. The average transmission power in the passband for the central frequencies of 0.9811 THz, 1.019 THz and 1.0395 THz, are 99.3%, 98.8% and 99.1%, respectively.

C. Bandwidth-Tunable Bandpass Filter

Finally, we consider a THz bandwidth-tunable bandpass filter, which also has the potential application in THz-wave circuits [42]. The design model of the filter is same as illustrated in Fig. 5. In this case, we only adjust the target bandwidth of the filter in the optimization process and keep other design

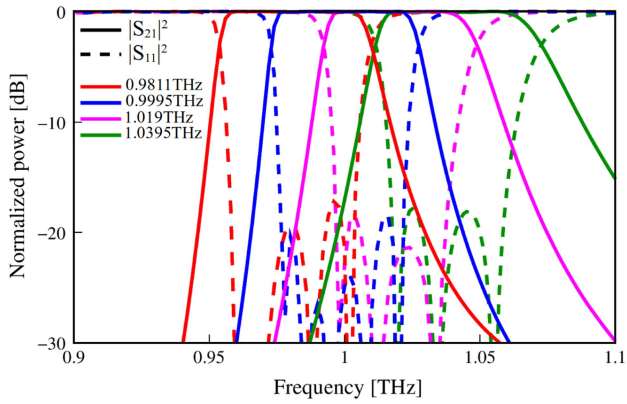

Fig. 10. Frequency characteristics of the optimized frequency-tunable bandpass filter at central frequency, 0.9811 THz, 0.9995 THz, 1.019 THz, and 1.0395 THz.

TABLE III
RANGE OF DESIGN VARIABLES AND OPTIMIZED PARAMETERS OF THE DESIGNED BANDWIDTH-TUNABLE BANDPASS FILTER WITH THE BANDWIDTH OF, 28 GHZ, AND 67 GHZ

Design variable	Variable range	Optimized parameter
BW = 28 GHz, CF = 0.9994 THz		
l_1	20 μm $\sim$ 100 μm	24.736 μm
l_2	20 μm $\sim$ $\lambda/2$	121.967 μm
l_3	20 μm $\sim$ 100 μm	99.980 μm
l_5	20 μm $\sim$ $\lambda/2$	150.000 μm
BW = 67 GHz, CF = 0.9995 THz		
l_1	20 μm $\sim$ 100 μm	36.206 μm
l_2	20 μm $\sim$ $\lambda/2$	127.613 μm
l_3	20 μm $\sim$ 100 μm	77.526 μm
l_5	20 μm $\sim$ $\lambda/2$	92.235 μm

parameters fixed as the first design example. Here, the target bandwidths are considered to be, 28 GHz and 68 GHz, and the target central frequency is set to 1 THz. The optimized parameters of the designed bandpass filter with different optimized bandwidths are shown in Table III. The obtained bandwidths are, 28 GHz, and 67 GHz with the optimized central frequency of, 0.9994 THz, and 0.9995 THz, respectively. The optimized structures show the desired behaviour with transmitting and rejecting the propagation fields within the passband and rejection band, respectively for different optimized bandwidths, as shown in Fig. 11. The frequency characteristics curves of the optimized devices with different bandwidths are depicted in Fig. 12. In the figure, it is shown that the optimized structures obtained the desired flat top transmission band at the targeted frequency range with different bandwidths. For the bandwidths of 28 GHz and 67 GHz, the average transmission power in the passband are, 98.5% and 99.6%, respectively.

IV. CONDUCTOR LOSS CALCULATION BY EIM

In the design optimization of the filters presented in the previous section, PEC is used as the parallel metal plates thus the conductor loss is not considered for those design examples. As in THz region conductor loss is not negligible, in this section we calculate the possible conductor loss to show the practical application of these designed bandpass filters. In this case we

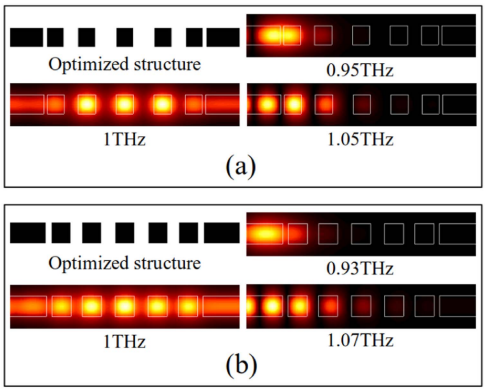

Fig. 11. Optimized structure and propagation fields in the optimized bandpass filter at different frequencies within passband and rejection band, (a) BW = 28 GHz and CF = 0.9994 THz, and (b) BW = 67 GHz and CF = 0.9995 THz.

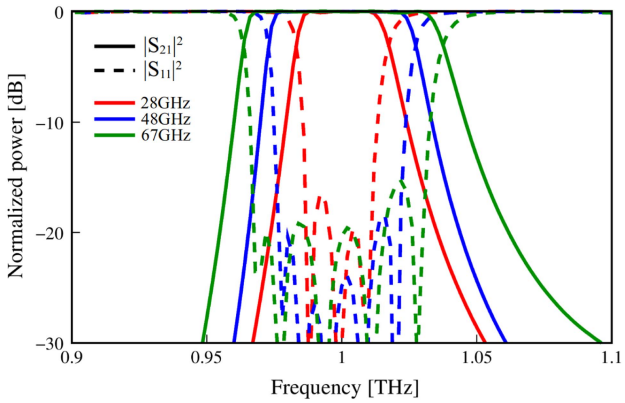

Fig. 12. Frequency characteristics of the optimized bandwidth-tunable bandpass filter with the bandwidth of, 28 GHz, 48 GHz, and 67 GHz.

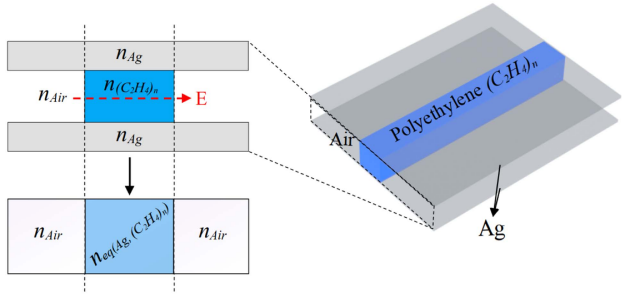

Fig. 13. Image of applying equivalent effective index method (EIM) to the NRD guide.

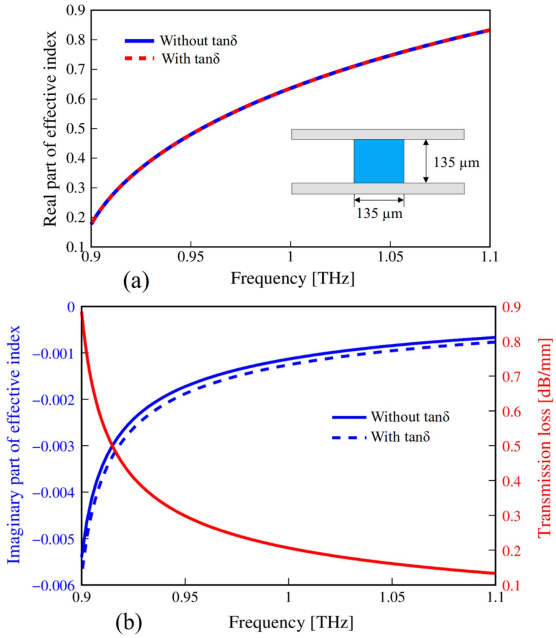

Fig. 14. Frequency response of the effective refractive index and the transmission performance of the NRD guide from LSM mode analysis, (a) Real part of effective index, (b) Imaginary part of effective index and transmission loss.

employed the EIM to the 2D-FVFEM to evaluate the transmission characteristics of the devices during the optimization process considering propagation loss due to the conductor plates. NRD guide confines almost all the power inside the dielectric strip without radiating or leaking into the air region, thus the propagation loss due to the conductor plates in the air region is negligible and core region is the responsible for the total conductor loss in the device. Therefore, we employed equivalent EIM only in the core region of the NRD grating bandpass filter. An image of applying equivalent effective index method to the NRD guide is shown in Fig. 13. Here, the core of the NRD guide device and two parallel conducting plates (Ag) are considered as a three-layer slab waveguide system. The equivalent refractive index is determined from the LSM mode analysis of the three-layer slab waveguide in a two-dimensional approximation analysis of the three-dimensional structure. In the analysis, the relative dielectric constant of Silver (Ag) is calculated by using Drude model [43] as follows:

$$\varepsilon_{\mathrm{Ag}} = 1 - \frac{\omega_p^2}{\omega^2 - j\omega\gamma} \tag{9}$$

where ω is the angular frequency, $\omega_p = 1.37 \times 10^{16}$ Hz is the bulk plasma frequency and $\gamma = 3.23 \times 10^{13}$ Hz is the electron collision frequency. Fig. 14 shows the frequency response of the effective refractive index and the transmission performance of the NRD guide from the LSM mode analysis. Here, the imaginary part of effective index with a dielectric loss tangent of polyethylene, $\tan\delta = 0.0001$ [32] is nearly close to that while not considering the $\tan\delta$, as seen in Fig. 14(b). Therefore, loss tangent of polyethylene does not have a significant effect on the transmission performance of the NRD guide as the dielectric loss in the NRD guide is very small compared to the conductor loss. In the Fig. 14(b), it is shown that the maximum transmission loss in the transmission band (0.95 THz - 1.07 THz) is only 0.3 dB/mm with a parallel metal plate (Ag) conductivity of 4.998×10^7 S/m. Here, the relative dielectric constant of polyethylene at 1 THz is, $\varepsilon_{(\mathrm{C_2H_4})n,\mathrm{EIM}} = 2.3 - j0.001442618$, where the imaginary part is calculated from the effective refractive index and represents the conductor loss in the NRD guide.

We consider the first design example with all the design parameters unchanged and optimize it again with EIM+2D-FVFEM to analyze the device performance with the conductor

TABLE IV
RANGE OF DESIGN VARIABLES AND OPTIMIZED PARAMETERS OF THE DESIGNED BANDPASS FILTER (OPTIMIZED WITH CONSIDERING CONDUCTOR LOSS)

Design variable	Variable range	Optimized parameter
l_1	20 μm $\sim$ 100 μm	41.807 μm
l_2	20 μm $\sim$ $\lambda/2$	125.180 μm
l_3	20 μm $\sim$ 100 μm	97.266 μm
l_5	20 μm $\sim$ $\lambda/2$	116.101 μm

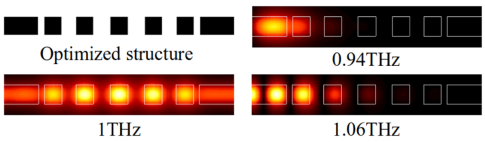

Fig. 15. Optimized structure and propagation fields in the optimized bandpass filter (optimized with considering conductor loss) at different frequencies.

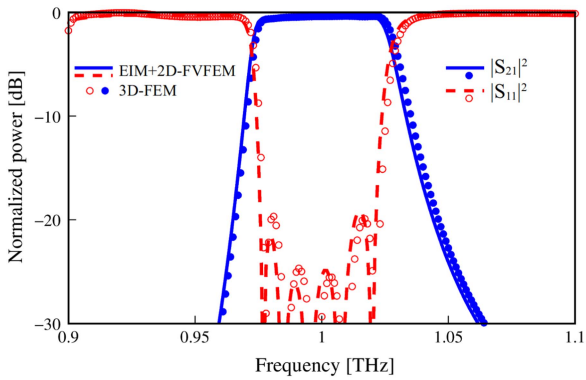

Fig. 16. Frequency characteristics of the optimized bandpass filter (optimized with considering conductor loss).

loss approximation. Table IV shows the optimized parameters of the designed bandpass filter after considering conductor loss. We can see, the optimized parameters are almost same and slightly changed due to the conductor loss consideration. Optimized structure and propagation fields in the optimized bandpass filter at different frequencies within passband and rejection band are shown in Fig. 15. Fig. 16 shows the frequency characteristics of the optimized bandpass filter. In the figure it is illustrated that, after conductor loss approximation also the device achieved almost ideal flat top transmission property. Here, the average insertion loss (IL) of the optimized device is only 0.46 dB in the passband, and the reflection in the passband is better than -20 dB. Then, we confirm the results obtained from the EIM and 2D-FVFEM analysis with the 3D analysis of the obtained structure. In this case, the frequency characteristics of the optimized structure is further calculated by the 3D-FEM. The EIM+2D-FVFEM results show high consistency with the 3D-FEM results, as seen in Fig. 16. Although transmission loss may be underestimated outside the core region, the difference between EIM+2D-FVFEM and 3D-FEM results is considerably small, thus the loss outside the core region is not significant and can be negligible. The numerical simulation time of the device using 3D-FEM is estimated 12 min. and 52 sec. with

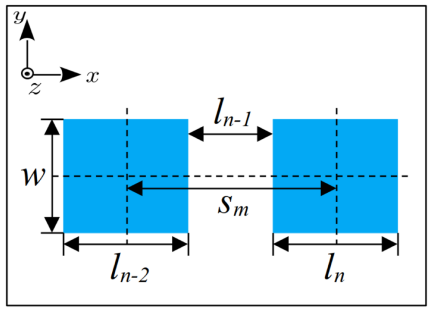

Fig. 17. Image of structural tolerance consideration of the optimized NRD grating filters.

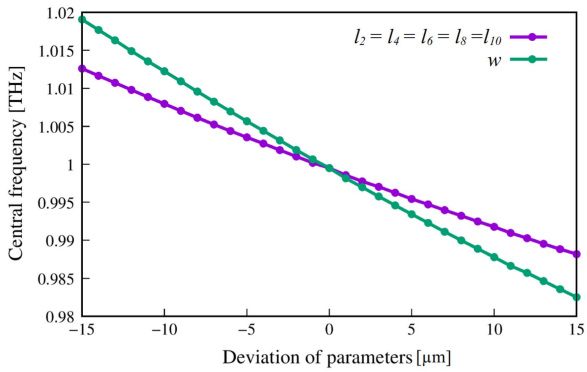

Fig. 18. Effect of design parameters (block lengths and width) deviation on the central frequency of the bandpass filter.

required computational memory of 305.6 GiB using a PC Intel(R) Xeon(R) Gold 6238R CPU @ 2.20 GHz, whereas the EIM and 2D-FVFEM analysis time at the same PC is only 13.52 sec. with 0.794 GiB of computational memory requirement. Therefore, we can see that utilizing EIM with 2D-FVFEM for conductor loss estimation significantly improves the design efficiency of the THz devices.

V. FABRICATION TOLERANCE

The THz NRD grating bandpass filters have been designed so far. In this section, the structural tolerance during the fabrication of these devices is discussed in terms of design parameters deviation effect on the bandwidth and central frequency. Here, block lengths and width are considered to be deviated, and keep center spacings, S_m $(m = 1, 2, 3, 4, 5, 6)$ and central position of the blocks fixed along x- and y-axis, respectively as shown in Fig. 17. In terms of block length deviation, it is considered that the block lengths, $l_n, l_{n-2}, .., l_{n-8}$ $(n = 10)$ become wider or narrower at the same time. Width, w for all the blocks is also considered to become wider or narrower at the same time, in case of width deviation consideration. The central frequency variation with the parameters deviation range within ± 15 μm is shown in Fig. 18. The variation in bandwidth is also investigated with the same parameters deviation range as shown in Fig. 19. In the Fig. 18, we can see the central frequency shifts downward with increase in block lengths and width, and shifts upward in

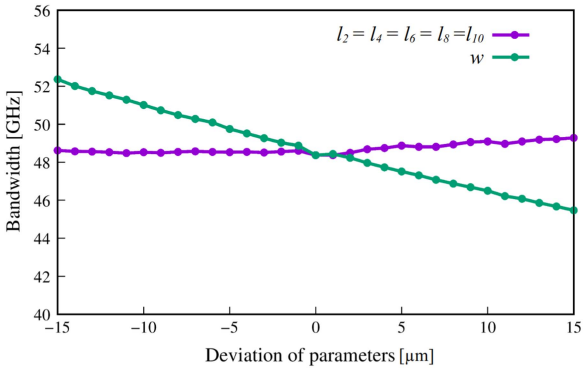

Fig. 19. Effect of design parameters (block lengths and width) deviation on the bandwidth of the bandpass filter.

both the cases while decreasing. The average central frequency shift is 0.814 GHz/μm length deviation and 1.217 GHz/μm width deviation. As shown in Fig. 19, with decreasing the block lengths, bandwidth almost remain unchanged, but it slightly increases while increasing block lengths. The bandwidth increases up to 52.367 GHz with 15 μm of block width decrease, and decreases up to 45.469 GHz with 15 μm of block width increase. Here, in terms of both the central frequency and bandwidth, width deviation is more sensitive than length deviation. Also, the parameters deviation is more sensitive to the central frequency than the bandwidth. If $\pm$ 2 GHz frequency shift is considerable, $(-3 \sim +2)\mu$m deviation in block lengths and $(-2 \sim +1)\mu$m deviation in block width may tolerable during the fabrication of the devices.

VI. Conclusion

In this paper, we proposed THz NRD grating bandpass filters and developed an efficient optimal design method to realize these devices based on GA and EIM. To show the usefullness of the design methodology and the effectiveness of the filters in the THz-band circuit applications, we designed several THz bandpass filters, single pass-band bandpass filter, frequency-tunable bandpass filter, and bandwidth-tunable bandpass filter. The proposed NRD grating bandpass filters achieved the desired flat top transmission property at the targeted frequency band. The proposed devices can achieve almost the ideal transmission property after considering propagation loss as well for practical application. The statement is confirmed by further optimizing the single pass-band bandpass filter taking conductor loss into account by EIM, where the desired flat top transmission band is achieved with only 0.46 dB of avg. IL and better than $-$ 20 dB of reflection in the passband. The optimized structure is further simulated by 3D-FEM and the obtained result agrees well with that of utilizing EIM and 2D-FVFEM. The proposed method shows high computational efficiency over 3D-FEM in terms of required computational time and memory. Furthermore, a thorough discussion of the fabrication tolerance of designed devices has also been conducted. In our future work, we would like to investigate more different types of NRD filters for THz applications and improve our design strategy.

References

[1] P. H. Siegel, "Terahertz technology," *IEEE Trans. Microw. Theory Tech.*, vol. 50, no. 3, pp. 910–928, Mar. 2002.
[2] R. Zhou, C. Wang, W. Xu, and L. Xie, "Biological applications of terahertz technology based on nanomaterials and nanostructures," *Nanoscale*, vol. 11, no. 8, pp. 3445–3457, 2019.
[3] P. H. Siegel, "Terahertz technology in biology and medicine," *IEEE Trans. Microw. Theory Tech.*, vol. 52, no. 10, pp. 2438–2447, Oct. 2004.
[4] Z. Chen et al., "Terahertz wireless communications for 2030 and beyond: A cutting-edge frontier," *IEEE Commun. Mag.*, vol. 59, no. 11, pp. 66–72, Nov. 2021.
[5] I. F. Akyildiz, J. M. Jornet, and C. Han, "Terahertz band: Next frontier for wireless commnuications," *Phys. Commun.*, vol. 12, pp. 16–32, 2014.
[6] B. Clough, J. Liu, and X. C. Zhang, ""All air-plasma" terahertz spectroscopy," *Opt. Lett.*, vol. 36, no. 13, pp. 2399–2401, 2011.
[7] J. F. Federici et al., "THz imaging and sensing for security applications–explosives, weapons and drugs," *Semicond. Sci. Technol.*, vol. 20, no. 7, pp. S266–S280, 2005.
[8] V. P. Wallace, E. MacPherson, J. A. Zeitler, and C. Reid, "Three-dimensional imaging of optically opaque materials using nonionizing terahertz radiation," *J. Opt. Soc. Amer. A*, vol. 25, no. 12, pp. 3120–3133, 2008.
[9] Y. A. Garcá-Jomaso, D. L. Hernández-Roa, J. Garduño-Mejáa, C. G. Treviño-Palacios, O. V. Kolokoltsev, and N. Qureshi, "Sub-wavelength continuous THz imaging system based on interferometric detection," *Opt. Exp.*, vol. 29, no. 12, pp. 19120–19125, 2021.
[10] B. Bowden, J. A. Harrington, and O. Mitrofanov, "Fabrication of terahertz hollow-glass metallic waveguides with inner dielectric coatings," *J. Appl. Phys.*, vol. 104, no. 9, 2008, Art. no. 093110.
[11] O. Mitrofanov and J. A. Harrington, "Dielectric-lined cylindrical metallic THz waveguides: Mode structure and dispersion," *Opt. Exp.*, vol. 18, no. 3, pp. 1898–1903, 2010.
[12] M. I. H. Patwary, A. Iguchi, and Y. Tsuji, "Efficient optimal design of mosaic-like PPDW devices for THz application using the adjoint variable method," *Opt. Exp.*, vol. 31, no. 10, pp. 16593–16606, 2023.
[13] G. K. C. Kwan and N. K. Das, "Excitation of a parallel-plate dielectric waveguide using a coaxial probe-basic characteristics and experiments," *IEEE Trans. Microw. Theory Techn.*, vol. 50, no. 6, pp. 1609–1620, Jun. 2002.
[14] T. Yoneyama and S. Nishida, "Nonradiative dielectric waveguide for millimeter-wave integrated circuits," *IEEE Trans. Microw. Theory Techn.*, vol. 29, no. 11, pp. 1188–1192, Nov. 1981.
[15] T. Yoneyama and S. Nishida, "Nonradiative dielectricwaveguide," in *Infrared and Millimeter Waves*, K. J. Button, Ed., Cambridge, MA, USA: Academic Press, 1984.
[16] J. Zhuang, W. Hong, and Z. Hao, "Design and analysis of a terahertz bandpass filter," in *Proc. IEEE Int. Wireless Symp.*, 2015, pp. 1–4.
[17] S. Song, F. Sun, Q. Chen, and Y. Zhang, "Narrow-linewidth and high-transmission terahertz bandpass filtering by metallic gratings," *IEEE Trans. Terahertz Sci. Technol.*, vol. 5, no. 1, pp. 131–136, Jan. 2015.
[18] H. Zhu, Y. Zhang, L. Ye, Y. Li, Y. Xu, and R. Xu, "On-chip terahertz bandpass filter based on substrate integrated plasmonic waveguide," *Results Phys.*, vol. 27, 2021, Art. no. 104553.
[19] J. He, P. Liu, Y. He, and Z. Hong, "Narrow bandpass tunable terahertz filter based on photonic crystal cavity," *Appl. Opt.*, vol. 51, no. 6, pp. 776–779, 2012.
[20] X. Ri-Hui and L. Jiu-Sheng, "Double-layer frequency selective surface for terahertz bandpass filter," *J. Infrared, Millimeter, Terahertz Waves*, vol. 39, no. 10, pp. 1039–1046, 2018.
[21] J. Li, Y. Li, and L. Zhang, "Terahertz bandpass filter based on frequency selective surface," *IEEE Photon. Technol. Lett.*, vol. 30, no. 3, pp. 238–241, Feb. 2018.
[22] T. Yeh et al., "Ultra-broad and sharp-transition bandpass terahertz filters by hybridizing multiple resonances mode in monolithic metamaterials," *Opt. Exp.*, vol. 20, no. 7, pp. 7580–7589, 2012.
[23] O. Paul, R. Beigang, and M. Rahm, "Highly selective terahertz bandpass filters based on trapped mode excitation," *Opt. Exp.*, vol. 17, no. 21, pp. 18590–18595, 2009.
[24] C. Chang, L. Huang, J. Nogan, and H. Chen, "Invited article: Narrowband terahertz bandpass filters employing stacked bilayer metasurface antireflection structures," *APL Photon.*, vol. 3, no. 5, 2018, Art. no. 051602.
[25] T. Yoneyama, F. Kuroki, and S. Nishida, "Design of nonradiative dielectric waveguide filters," *IEEE Trans. Microw. Theory Tech.*, vol. MTT- 32, no. 12, pp. 1659–1662, Dec. 1984.

[26] Y. Ping and M. J. Feng, "An investigation of NRD waveguide grating," in *Proc. IEEE MTT-S Int. Microw. Symp. Dig.*, 1989, pp. 499–502.
[27] J. A. Monsoriu, B. Gimeno, E. Silvestre, and M. V. Andres, "Analysis of inhomogeneously dielectric filled cavities coupled to dielectric-loaded waveguides: Application to the study of NRD-guide components," *IEEE Trans. Microw. Theory Techn.*, vol. 52, no. 7, pp. 1693–1701, Jul. 2004.
[28] H. Hanen, L. Lassaad, G. Ali, and G. Abdelhafedh, "Effect of the width of the NRD waveguide on the s. parameter of a pass band filter," *J. Electromagn. Anal. Appl.*, vol. 4, no. 10, 2012, Art. no. 423.
[29] D. Li, P. Yang, and K. Wu, "An order-reduced volume-integral equation approach for analysis of NRD-guide and H-guide millimeter-wave circuits," *IEEE Trans. Microw. Theory Techn.*, vol. 53, no. 3, pp. 799–812, Mar. 2005.
[30] Y. Tsuji, K. Morimoto, A. Iguchi, T. Kashiwa, and S. Nishiwaki, "Two-dimensional full-vectorial finite element analysis of NRD guide devices," *IEEE Micro. Wireless Compon. Lett.*, vol. 31, no. 4, pp. 345–348, Apr. 2021.
[31] K. Zhou et al., "Transmittance of high-density polyethylene from 0.1 THz to 15 THz," *Proc. SPIE*, vol. 11196, pp. 144–149, 2019.
[32] F. Kuroki, H. Ohta, and T. Yoneyama, "Transmission characteristics of NRD guide as a transmission medium in THz frequency band.," in *Proc. IEEE Joint 30th Int. Conf. Infrared Millimeter Waves 13th Int. Conf. Terahertz Electron.*, 2005, pp. 331–332.
[33] D. Whitley, "A genetic algorithm tutorial," *Statist. Comput.*, vol. 4, no. 2, pp. 65–85, 1994.
[34] J.-F. Lee, D.-K. Sun, and Z. J. Cendes, "Full-wave analysis of dielectric waveguides using tangential vector finite elements," *IEEE Trans. Microw. Theory Techn.*, vol. 39, no. 8, pp. 1262–1271, Aug. 1991.
[35] M. Koshiba and Y. Tsuji, "Curvilinear hybrid edge/nodal elements with triangular shape for guided-wave problems," *J. Lightw. Technol.*, vol. 18, no. 5, pp. 737–743, May 2000.
[36] N. Hieda, K. Morimoto, A. Iguchi, Y. Tsuji, and T. Kashiwa, "Topology optimal design of NRD guide devices using function expansion method and evolutionary approaches," *IEICE Trans. Electron.*, vol. 105, no. 11, pp. 652–659, 2022.
[37] N. Hansen and A. Ostermeier, "Adapting arbitary normal mutation distributions in evolution strategies: The covariance matrix adaptation," in *Proc. IEEE Int. Conf. Evol. Computation*, 1996, pp. 312–317.
[38] Y. Yao, X. Cheng, S. Qu, J. Yu, and X. Chen, "Graphene–metal based tunable band–pass filters in the terahertz band," *IET Microwaves, Antennas Propag.*, vol. 10, no. 14, pp. 1570–1575, 2016.
[39] Y. Zhu et al., "Tunable dual-band terahertz metamaterial bandpass filters," *Opt. Lett.*, vol. 38, no. 14, pp. 2382–2384, 2013.
[40] G. C. Ram, P. Sambaiah, S. Yuvaraj, and M. V. Kartikeyan, "Graphene based tunable bandpass filter for terahertz spectroscopy of polymers," *Optik*, vol. 268, 2022, Art. no. 169792.
[41] X. Lv, R. T. Ako, M. Bhaskaran, S. Sriram, C. Fumeaux, and W. Withayachumnankul, "Frequency-selective-surface-based mechanically reconfigurable terahertz bandpass filter," *IEEE Trans. THz Sci. Technol.*, vol. 12, no. 3, pp. 257–266, May 2022.
[42] J. Huang et al., "Active controllable bandwidth of THz metamaterial bandpass filter based on vanadium dioxide," *Opt. Commun.*, vol. 465, 2020, Art. no. 125616.
[43] Y. Cao, K. Nallappan, H. Guerboukha, G. Xu, and M. Skorobogatiy, "Additive manufacturing of highly reconfigurable plasmonic circuits for terahertz communications," *Optica*, vol. 7, no. 9, pp. 1112–1125, 2020.